A New Look at the Ylidic Bond in Phosphorus Ylides and Related Compounds: Energy Decomposition Analysis Combined with a Domain-Averaged Fermi Hole Analysis

Maria José Calhorda,*,† Andreas Krapp,‡ and Gernot Frenking*,‡

Departamento de Química e Bioquímica, Faculdade de Ciências, Universidade de Lisboa, 1749-016 Lisboa, Portugal, and Fachbereich Chemie, Philipps-Universität Marburg, Hans-Meerwein-Strasse, D-35043 Marburg, Germany

Received: December 15, 2005; In Final Form: February 8, 2007

Geometries and bond dissociation energies of the ylide compounds H_2CPH_3, H_2CPMe_3, H_2CPF_3, $(BH_2)_2CPH_3$, H_2CNH_3, H_2CAsH_3, H_2SiPH_3, and $(BH_2)_2SiPH_3$ have been calculated using ab initio (MP2, CBS-QB3) and DFT (B3LYP, BP86) methods. The nature of the ylidic bond $R_2E^1-E^2X_3$ was investigated with an energy decomposition analysis and with the domain-averaged Fermi hole (DAFH) analysis. The results of the latter method indicate that the peculiar features of the ylidic bond can be understood in terms of donor−acceptor interactions between closed-shell R_2E^1 and E^2X_3 fragments. The DAFH analysis clearly shows that there are two bonding contributions to the ylidic bond. The strength of the donor and acceptor contributions to the attractive orbital interactions can be estimated from the energy decomposition analysis (EDA) calculations, which give also the contributions of the electrostatic attraction and the Pauli repulsion of the chemical bonding. The EDA and DAFH results clearly show that the orbital interactions take place through the singlet ground state of the R_2E^1 fragment where the donor orbital of E^1 yields π-type back-donation while the E^2X_3 lone-pair orbital yields σ-type bonding. Both bonds are polarized toward E^2X_3 when $E^2 = P$, while the σ-type bonding remains more polarized at E^2X_3 when $E^2 = N$, As. This shows that the phosphorus ylides exhibit a particular bonding situation which is clearly different from that of the nitrogen and arsenic homologues. With ylides built around a P−C linkage, the π-acceptor strength of phosphorus and the σ-acceptor strength at carbon contribute to a double bond which is enhanced by electrostatic contributions. The strength of the σ and π components and the electrostatic attraction are then fine-tuned by the substituents at C and P, which yields a peculiar type of carbon−phosphorus bonding. The EDA data reveal that the relative strength of the ylidic bond may be determined not only by the $R_2E^1 \rightarrow E^2X_3$ π back-donation, but also by the electrostatic contribution to the bonding. The calculations of the $R_2E^1-E^2X_3$ bond dissociation energy using ab initio methods predict that the order of the bond strength is $H_2C-PMe_3 > H_2C-PF_3 > H_2C-PH_3 > (BH_2)_2C-PH_3 > H_2C-AsH_3 > H_2C-NH_3 \sim H_2Si-PH_3 \sim (BH_2)_2Si-PH_3$. The DFT methods predict a similar trend, but they underestimate the bond strength of $(BH_2)_2CPH_3$.

Introduction

The many applications of phosphorus ylides in synthesis have contributed to a wide interest in the nature of their bonding and their chemical properties.[1,2] Numerous geometries of phosphorus ylides have been determined by single-crystal X-ray diffraction.[3−5] For the simplest ylide structurally characterized, H_2CPMe_3, there are two sets of geometrical parameters available from electron diffraction and X-ray data.[6] In the latter compound, the fragments PMe_3 (a closed-shell molecule) and CH_2 (a carbene with a triplet ground state) are bonded to each other, yielding a bonding which is not easy to describe using conventional bonding models. Using valence bond (VB) models, the contribution of two resonance hybrids (Scheme 1) has been suggested in an early study to explain the P−C double-bond character.[7] The bonding in ylides may alternatively be described in terms of donor−acceptor interactions within the framework of molecular orbital (MO) theory (Scheme 1). The back-donation from occupied orbitals of the carbene fragment into vacant orbitals of the phosphane molecule should lengthen the in-plane P−X bond more than the out-of-plane bonds.

SCHEME 1: Schematic Representation of C−P Bonding in Phosphorus Ylides: (a) VB Resonance Structures; (b) MO Donor−Acceptor Model[a]

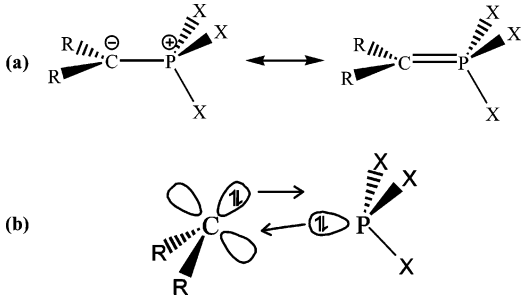

[a] The antibonding (π^*) PX_3 acceptor orbital is not shown here.

Several computational studies of simple ylidic species have been carried out in recent years.[8,10−15] The nature of the P−C bond was addressed at correlated levels of theory and considered to be a double bond, similar in character to the classical $HP{=}CH_2$ bond, based on the comparison of rotational barriers and bond strengths.[8] The results of an atom-in-molecule (AIM) analysis[9] and the association of basins to each atom belonging

† Universidade de Lisboa.
‡ Philipps-Universität Marburg.

10.1021/jp057320v CCC: $37.00
Published on Web 03/24/2007

CHART 1: Calculated Conformations of the Ylides $R_2E^1-E^2X_3$ a and b[a]

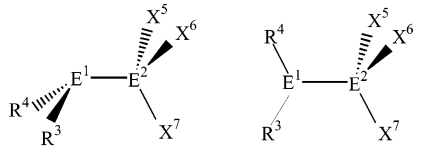

[a] Note that the mirror plane of the C_s symmetry in conformation **a** bisects the E^1-R_2 plane while in conformation **b** the E^1-R_2 plane is in the mirror plane.

to a molecule have been used by Mitrasinovic for the interpretations of bonds in ylide compounds.[10] Important contributions to the understanding of the chemical bond in ylides have been published by Dobago et al.[11,12] A comparison of the H_2C-EH_3 bonds (E = N, P, As) was performed based on delocalization indices obtained from an AIM analysis.[11] The N−C bond was considered to be weaker than a single bond, but for P and As a polar interaction was assigned, with the strength of the bond depending on electrostatic interactions and negative hyperconjugation. Theoretical investigations about electron-poor phosphorus ylides were reported by Nguyen and co-workers.[13] AIM and ELF investigations have been published in two theoretical studies by Silvi and co-workers[14] and by Savin et al.[15] Reviews about the bonding in main-group compounds show that ylidic bonds are usually discussed in terms of negative hyperconjugation where the P−C bond order in the compounds is determined by the substituents.[16,17]

In this work, we examine the bonding in the parent phosphorus ylide H_2CPH_3 (**1**) and in the substituted analogues H_2CPMe_3 (**2**), H_2CPF_3 (**3**), and $(BH_2)_2CPH_3$ (**4**) using an energy decomposition analysis[18−20] (EDA) and the analysis of domain-averaged Fermi holes (DAFH).[21−24] We also investigate the heteroatom analogues H_2CNH_3 (**5**), H_2CAsH_3 (**6**), H_2SiPH_3 (**7**), and $(BH_2)_2SiPH_3$ (**8**). The results offer a quantitative insight into the nature of the bonding which comes from energy and charge partitioning methods that do not depend on an orbital partitioning scheme. We theoretically predict bond energies of the ylides **1**−**8** using high-level CBS-QB3 calculations.

Methods

Geometry optimizations were first performed with DFT using the hybrid functional B3LYP[25−27] and Møller−Plesset perturbation theory terminated at second order (MP2)[28] in combination with correlation consistent triple-ζ basis sets augmented by a set of diffuse functions (aug-cc-pVTZ)[29] using the Gaussian03 program.[30] Standard SCF and geometry-optimization criteria were applied, and the standard integration grid was used in the DFT calculations. In the MP2 calculations, the core electrons of the second- and third-row atoms were not correlated. The nature of the stationary points was examined by calculating the Hessian matrix at the corresponding levels of theory. Improved dissociation energies were calculated using the CBS-QB3[31] extrapolation scheme as implemented in Gaussian03.

To analyze the ylidic bonds with the EDA, we also optimized the geometries with the ADF2003.1 program[20,32−34] using the BP86[35,36] exchange-correlation functional in combination with a basis set of triple-ζ quality augmented by two sets of polarization functions[37,38] (BP86/TZ2P). In the ADF calculations the zero-order regular approximation (ZORA)[39] was used to deal with scalar relativistic effects and the core electrons were treated by the frozen-core approximation[40] (for B−F, $(1s)^2$; for Si and P, $(1s2s2p)^{10}$; for As, $(1s2s2p3s3p)^{18}$). ADF uses an auxiliary set of s, p, d, f, and g Slater-type orbitals to fit the molecular density and to represent the Coulomb and exchange potentials in each SCF cycle.[41]

The nature of the $R_2E^1-E^2X_3$ binding interactions was investigated with the energy decomposition analysis of ADF.[20] The EDA was originally developed by Morokuma[18] and later modified by Ziegler and Rauk.[19] The focus of the bonding analysis is the instantaneous interaction energy, ΔE_{int}, of the bond, which is the difference between the energy of the molecule and the energy of the fragments in the frozen geometry of the compound. The interaction energy can be divided into three main components:

$$\Delta E_{int} = \Delta E_{elstat} + \Delta E_{Pauli} + \Delta E_{orb} \quad (1)$$

ΔE_{elstat} gives the electrostatic interaction energy between the fragments, which is calculated using the frozen electron density distribution of the fragments R_2E^1 and E^2X_3 in the geometry and the electronic reference state of the molecules $R_2E^1-E^2X_3$. The second term in eq 1, ΔE_{Pauli}, refers to the repulsive interactions between the fragments, which are caused by the fact that two electrons with the same spin cannot occupy the same region in space. ΔE_{Pauli} is calculated by enforcing the Kohn−Sham determinant of the orbitals of the superimposed fragments to obey the Pauli principle by antisymmetrization and renormalization. The stabilizing orbital interaction term, ΔE_{orb}, is calculated in the final step of the energy partitioning analysis when the Kohn−Sham orbitals relax to their optimal form. This term can be further partitioned into contributions by the orbitals belonging to different irreducible representations of the point group of the interacting system. The interaction energy, ΔE_{int}, can be used to calculate the bond dissociation energy, D_e, by adding ΔE_{prep}, which is the energy necessary to promote the fragments from their equilibrium geometry to the geometry in the compounds (eq 2). Further details of the energy partitioning analysis can be found in the literature.[20]

$$-D_e = \Delta E_{prep} + \Delta E_{int} \quad (2)$$

The electronic structure of the ylides was analyzed with the domain-averaged Fermi holes (DAFH)[21−24] method, which was introduced by Ponec as an interpretative tool to elucidate the bonding in molecules. The DAFH method is based on an analysis of the correlation hole defined as the difference between the first- and second-order densities ($\rho(r_1)$ and $\rho(r_1,r_2)$), which is integrated over a defined region of space, called the domain Ω, and averaged by the population N of the domain Ω. This leads to the domain-averaged hole g_Ω:

$$g_\Omega = N_\Omega \rho(r_1) - 2 \int_\Omega \rho(r_1,r_2)\, dr_1$$

The correlation hole can be divided in the Coulomb hole and the Fermi hole, which comes from the interaction of electrons having the same spin in the domain Ω. Following the suggestion of Ponec,[22] we have chosen for the domain Ω the atomic basins which are defined through the topological analysis of the electron density where the boundaries are given by the zero-flux surfaces.[9] Ponec could show that with this choice the DAFH method yields information about the valence state of an atom (or a group of atoms) in a molecule. To this end Ponec diagonalized the matrix representation of the correlation hole g_Ω in the basis of the atomic orbitals used to build the wave function, followed by an isopygnic transformation of the eigenvectors associated with nonzero eigenvalue values.[21−24] The chemical bonds, core pairs, and lone pairs within the domain

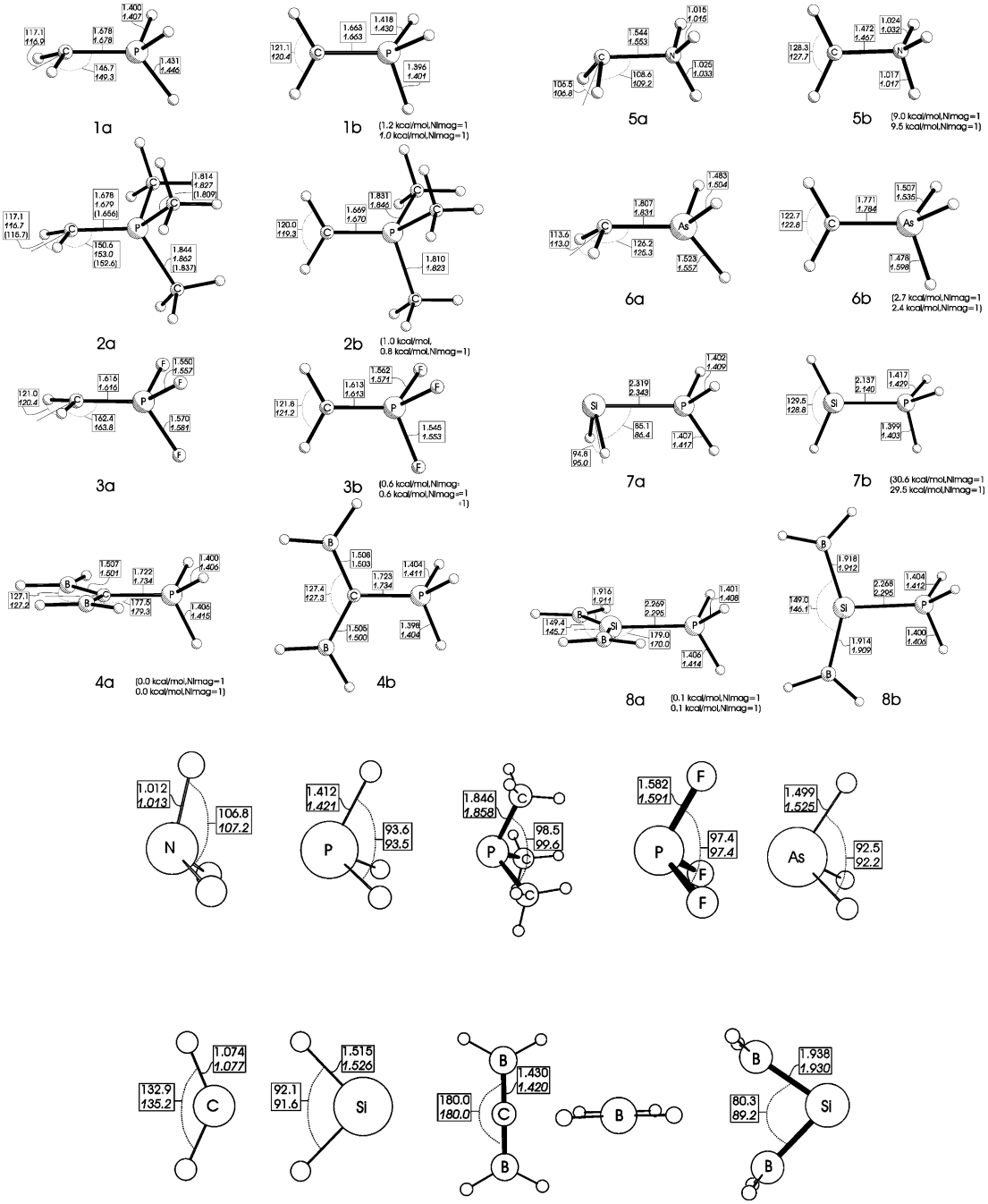

Figure 1. Optimized geometries of the ylides $R_2E^1-E^2X_3$ (**1**−**8**) and the fragments R_2E^1 and E^2X_3 in the electronic ground state. The upper values come from MP2/aug-cc-pVTZ, and the lower values in italics come from B3LYP/aug-cc-pVTZ calculations. The experimental values for **2a** are given in parentheses. They have been taken from ref 6. Distances in angstroms and angles in degrees.

Ω are represented by the eigenvectors of the hole associated with eigenvalue values close to 2. The number of free valences of a fragment can be identified with the number of nonzero eigenvalue values whose numerical values are significantly different from 2. The eigenvalues close to 1 can be identified as unpolar covalent bonds connecting two fragments. Visual inspection of the shape gives insight into the nature of the eigenvectors.

The DAFH analysis in the present work was performed with the WBader program of Ponec,[42] which uses as input the atomic overlap matrix (AOM) calculated by the AIMPAC program of Bader[43] and a Gaussian98[44] output file. We used the B3LYP/aug-cc-pVTZ densities for the DAFH analysis. GaussView3.0 was used to visualize the DAFH eigenvectors.

Geometries and Bond Energies

We optimized the geometries of $R_2E^1-E^2X_3$ (**1**−**8**) with C_s symmetry constraints using two different conformations denoted **a** and **b**, which are shown in Chart 1. In conformation **a**, the substituents at the carbene or silylene group are staggered with respect to the E^2X_3 moiety, while in **b** one E−R bond of the planar ER_2 group eclipses the E^2-X_7 bond. Figure 1 gives the most important bond lengths and angles of the optimized structures **1**−**8** and the relative energies of the **a** and **b** conformations, calculated at the MP2/aug-cc-pVTZ and B3LYP/aug-cc-pVTZ levels of theory. The optimized geometries of the fragments R_2E^1 and E^2X_3 in the electronic ground state (triplet state for CH_2, singlet state for the other molecules) are also shown.

TABLE 1: Calculated Dissociation Energies D_e (D_0) (in kcal/mol) for the Dissociation of $R_2E^1-E^2X_3$ (R = H, BH_2; E^1 = C, Si; E^2 = N, P, As; X = H, Me, F) in Fragments R_2E^1 and E^2X_3 in the Electronic Ground State

		B3LYP/aug-cc-pVTZ		BP86/TZ2P		MP2/aug-cc-pVTZ		CBS-QB3
$R_2E^1-E^2X_3$	no.	D_e	D_0	D_e	D_0[a]	D_e	D_0	D_0
CH_2PH_3	**1a**	53.85	47.84	57.17	51.16	59.45	53.38	53.87
CH_2PMe_3	**2a**	69.17	64.13	72.97	67.93	77.12	73.48[a]	72.60
CH_2PF_3	**3a**	65.49	60.06	68.26	62.83	74.32	69.06	71.26
$C(BH_2)_2PH_3$	**4b**	30.65	25.07	31.46	25.88	51.92	46.07	39.41
CH_2NH_3	**5a**	27.04	19.90	28.39	21.25	28.77	21.40	22.32
CH_2AsH_3	**6a**	36.54	31.18	37.06	31.70	46.08	40.67	35.42
SiH_2PH_3	**7a**	23.19	19.32	26.95	23.08	27.68	23.72	22.21
$Si(BH_2)_2PH_3$	**8b**	19.01	15.63	25.30	21.92	27.71	24.21	21.15

[a] Zero point energy correction at B3LYP/aug-cc-pVTZ.

Our calculated geometries of **1**−**8** agree quite well with previously reported theoretical data.[8,10−15] The calculated values for the bond lengths and angles of H_2CPMe_3 (**2a**) are also in good agreement with the gas-phase data which have been obtained from electron diffraction measurements[6] given in Figure 1. The excellent agreement for the bending angle of the CH_2 moiety between theory (151° and 153°) and experiment (152.6°) must not be overinterpreted, because the latter value is mainly the result of restraints in the GED analysis and thus represents almost pure theoretical information.[6]

Conformations **a** are energy minima (i = 0) for structures **1**−**3** and **5**−**7** while conformations **b** of the latter molecules are transition states (i = 1). For compounds **4** and **8** of the molecules $R_2E^1-E^2X_3$, which have π-acceptor substituents R= BH_2, the conformations **b** are energy minima but they are only marginally lower in energy (<0.1 kcal/mol) than conformations **a** (Figure 1). Please note that atom E^1 of $R_2E^1-E^2X_3$ compounds **4** and **8** is planar or nearly planar coordinated in both conformations **a** and **b**. There is a significant difference between the equilibrium geometries of the $H_2E^1-E^2X_3$ compounds **1a**−**3a**, **5a**−**7a** and the π-acceptor-substituted compounds **4** and **8**. The former molecules have a pyramidal arrangement at atom E^1, while the latter species have planar coordinated atoms E^1. The calculated value for the pyramidal angle shows a large variation from ∼85° in H_2Si-PH_3 to ∼109° in H_2C-NH_3, ∼126° in H_2CAsH_3, 147°−162° in H_2CPX_3, and 180° in $(BH_2)_2E^1-PH_3$. Another interesting observation concerns the E^2-X bond lengths of $R_2E^1-E^2X_3$ in the conformations **a** and **b**. In structures **1a**−**8a**, the E^2-X bond, which is in the mirror plane bisecting the R_2E^1 moiety (E^2-X_7 in Chart 1), is always longer than the other two E^2-X bonds. In contrast to this the unique E^2-X_7 bond of structures **1b**−**8b** which is lying in the mirror plane is always shorter than the other two E^2-X bonds. The results are in agreement with the MO bonding model shown in Scheme 1. This will be discussed in the section about the bonding.

A comparison of the geometries of the ylides $R_2E^1-E^2X_3$ with the free fragments R_2E^1 and E^2X_3 shows (Figure 1) that some E^2-X bonds become longer in the ylides while others become shorter. We want to point out that the geometry of the free carbene $C(BH_2)_2$, which has a linear B−C−B arrangement, is significantly different from that of free $Si(BH_2)_2$. The calculated results of the latter species are in agreement with previous investigations.[45−47]

The energy differences ΔE between conformers **a** and **b** are small for most compounds (ΔE < 2.7 kcal/mol), except for **5** (ΔE = 9.0 and 9.5 kcal/mol) and particularly **7** (ΔE = 30.6 and 29.5 kcal/mol), which have strongly pyramidal $H_2E^1-E^2$ moieties. It is gratifying that the bond lengths and angles and the relative energies of conformers **a** and **b** calculated at MP2/aug-cc-pVTZ and B3LYP/aug-cc-pVTZ agree quite well with each other. Both methods predict that the E^1-E^2 bond length in the conformers **b** is always shorter than in the conformers **a**, and yet the latter conformation is lower in energy in the cases of **1**−**3** and **5**−**7** than the former.

TABLE 2: Wiberg Bond Orders $P(E^1-E^2)$ and NBO Partial Charges at B3LYP/aug-cc-pVTZ

$R_2E^1-E^2X_3$	no.	$P(E^1-E^2)$	$q(E^1)$	$q(E^2)$	$q(E^1R_2)$
CH_2PH_3	**1a**	1.372	−1.15	0.85	−0.71
CH_2PMe_3	**2a**	1.332	−1.22	1.51	−0.78
CH_2PF_3	**3a**	1.517	−1.26	2.35	−0.74
$C(BH_2)_2PH_3$	**4b**	1.107	−1.27	0.93	−0.92
CH_2NH_3	**5a**	0.864	−0.73	−0.69	−0.46
CH_2AsH_3	**6a**	1.279	−1.10	0.84	−0.69
SiH_2PH_3	**7a**	0.805	0.13	0.26	−0.29
$Si(BH_2)_2PH_3$	**8b**	0.817	0.18	0.30	−0.38

Table 1 gives the calculated values for the bond dissociation energy (BDE) of the E^1-E^2 bonds of **1**−**8** at four different levels of theory. The CBS-QB3 data shall be used as reference for the values which are predicted at B3LYP, BP86, and MP2. The BDE values are calculated as energy differences between the molecules $R_2E^1-E^2X_3$ and the optimized fragments R_2E^1 and E^2X_3 in their electronic ground state, i.e., triplet ($^3B_1$) state of CH_2 and singlet state for the other fragments.

The R_2C-PX_3 bonds of **1**−**4** are quite strong, but the BDE of the π-acceptor-substituted compound $(BH_2)_2C-PH_3$ (**4b**) is clearly lower than the values for **1**−**3** (Table 1). The DFT values for the bond energies are smaller than the ab initio values, particularly for **4b**. The MP2 results suggest the following trend for the BDE: **2** > **3** > **1** > **4** > **6** > **8** ∼ **7** > **5**. The same trend is predicted for the calculated molecules at CBS-QB3 except that compounds **5**, **7**, and **8** have nearly the same (small) BDE. The DFT values show a similar trend, and the absolute values for the BDE are comparable to the CBS-QB3 data with the notable exception of **4b**. B3LYP and BP86 significantly underestimate the bond strength of $(BH_2)_2C-PH_3$.

Bonding Analysis

We used various methods for elucidating the bonding in the ylides $R_2E^1-E^2X_3$ (**1**−**8**). Useful information comes from the calculated Wiberg bond indices[48] and the partial charges, which are given in Table 2.

The calculated bond orders $P(E^1-E^2)$ shown in Table 2 will be compared with typical values for E^1-E^2 single bonds in the compounds H_3C-PH_2 (1.013), H_3C-NH_2 (1.035), H_3C-AsH_2 (0.969), and H_3Si-PH_2 (0.993), which are close to the value 1.[49] The data for **1**−**8** suggest that there is some double-bond character in H_2C-PF_3 (**3a**) and to a lesser extent in H_2C-PH_3 (**1a**), H_2C-PMe_3 (**2a**), and H_2C-AsH_3 (**6a**), while the double-bond character in $(BH_2)_2C-PH_3$ (**4b**) is rather small. The $P(E^1-E^2)$ values of H_2C-NH_3 (**5a**), H_2Si-PH_3 (**7a**), and $(BH_2)_2Si-PH_3$ (**8b**) are even smaller than those for a typical single bond

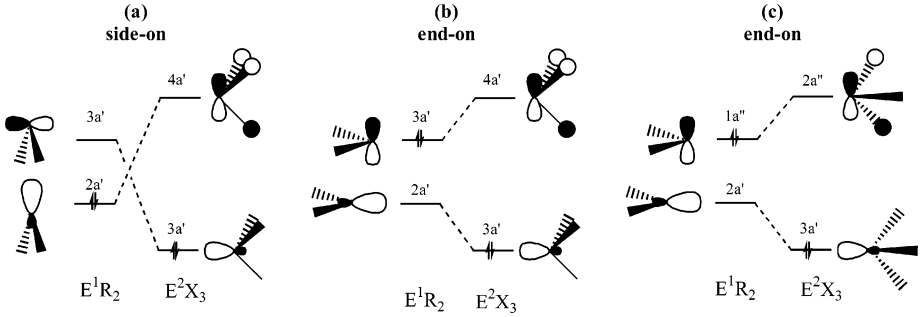

Figure 2. Orbital interaction diagram between the frontier orbitals of E^1R_2 and E^2X_3 fragments for the side-on and end-on bonding models. (a) Side-on approach between E^1R_2 in the singlet ground state and E^2X_3 in conformation **a**. (b) End-on approach between E^1R_2 in the doubly excited singlet state and E^2X_3 in conformation **a**. (c) End-on approach between E^1R_2 in the doubly excited singlet state and E^2X_3 in conformation **b**. For conformations **a** and **b** see Chart 1.

in the reference compounds. The R_2E^1 fragment of $R_2E^1-E^2X_3$ always carries a negative partial charge, although the silicon atoms in **7a** and **8b** have a small positive charge. Note that the phosphorus atoms in the latter compounds are even more positively charged than the silicon atoms, although P is more electronegative than Si. In short, there is always a charge donation in the direction $R_2E^1 \leftarrow E^2X_3$.

More details about the bonding are available from the EDA investigation. A crucial step for the EDA of compounds $R_2E^1-E^2X_3$ is the choice of the electronic states for the interacting fragments R_2E^1 and E^2X_3. CH_2 has a ($^3B_1$) electronic ground state which is 9.6 kcal/mol lower in energy than the ($^1A_1$) first excited singlet state.[50] The other R_2E^1 and E^2X_3 fragments have singlet ground states. The electronic structures of singlet **1**−**8** can be built from two triplet or two singlet fragments. Calculations showed that the preparation energy of the fragments from the electronic ground states into two triplet species was always significantly higher than that for the formation of two singlet states, which are described below. Also, the EDA calculations using triplet fragments give in most cases much higher values for the orbital interaction term, which indicates that the singlet states are a better description for the bonding situation of the ylides. Only in the case of the H_2C-PR_3 ylides **1**−**3** has the ΔE_{orb} term similar values for the interactions between singlet and triplet fragments, which indicates that the discussion of the intrinsic bonding situation in the latter compounds in terms of electron-sharing bonds is a reasonable approach. For the other molecules the EDA results clearly show that the model of orbital interactions between singlet fragments is clearly favored over the triplet interactions model. To compare the compounds using the same type of interacting fragments, we discuss only the EDA results using a donor−acceptor approach to the chemical bonding in **1**−**8**. The EDA results for the interactions between triplet fragments are given in Table S2 of the Supporting Information.

We want to point out that there is an important difference between conformations **a** and **b**, which both have C_s symmetry. The lone-pair donor orbital and the empty acceptor p orbital at atom E^1 in **a** are lying in the mirror plane, which means that donation and back-donation (see the MO model shown in Scheme 1b) both involve orbitals having a′ symmetry and cannot be distinguished through an orbital symmetry analysis. In conformation **b**, however, the E^1 lone-pair orbital has a″ symmetry because the mirror plane bisects the p(π) orbital. Therefore, $R_2E^1 \leftarrow E^2X_3$ donation and $R_2E^1 \rightarrow E^2X_3$ back-donation can now become distinguished because the former interactions come from orbitals having a′ symmetry, while the latter have a″ symmetry. This is important for the EDA method, which requires appropriate symmetry in order to distinguish between different orbital interactions.

Figure 2 shows schematically the arrangements of the fragments in the singlet states which have been used for the calculations. In the side-on model (Figure 2a) the R_2E^1 fragment is in the lowest lying singlet state where the HOMO is the lone-pair σ orbital and the LUMO is the p(π) orbital. In $R_2E^1-E^2X_3$, the latter becomes the acceptor orbital for the lone-pair σ MO of E^2X_3, while the former donates electronic charge into the vacant π^* orbital of E^2X_3. Note that the symmetry assignments σ and π are given with respect to the symmetry of the respective fragments. The side-on model should be appropriate for ylides $R_2E^1-E^2X_3$, which have a strongly pyramidal arrangement at atom E^1. In the end-on model (Figure 2b), the R_2E^1 fragment has a doubly occupied p(π) orbital at E as HOMO, while the LUMO is the sp^2-type σ orbital; i.e., HOMO and LUMO have exchanged electronic occupation with respect to the lowest lying singlet state. Although the end-on model uses an electronically excited state of R_2E^1 as reference state, it is the appropriate model for ylides that have planar or nearly planar environment about E^1. Figure 2a,b shows the arrangement of the fragments using conformation **a**, which is an energy minimum for compounds **1**−**3** and **5**−**7**. Figure 2c uses the same electronic states as in Figure 2b but the arrangement of the E^2X_3 fragment with respect to the R_2E^1 moiety is different, yielding conformation **b**.

Table 3 gives the EDA results for the carbon−phosphorus ylides **1**−**4** using different arrangements of the interacting fragments which are displayed in Figure 2. The results for the side-on model of **1a** show that the Pauli repulsion between CH_2 in the lowest lying singlet state and E^2X_3 is very large, because the lone-pair orbitals of the fragments are pointing toward each other. The end-on model for **1a** has much less Pauli repulsion, but also the value for the orbital term ΔE_{orb} is much less than that using the side-on model. This means that the molecular orbitals of the fragments using the excited singlet state of CH_2 are better suited for modeling the electronic structure of **1a** than those using the ground state. This result supports the use of the end-on model for analyzing the carbon−phosphorus bond in **1b**. Table 3 shows that the orbital interactions in **1b** as in **1a** are much more important for the binding interactions than the electrostatic attraction. The most important result concerns the strength of the $H_2C \rightarrow PH_3$ π back-donation in **1b**, which is given by the contributions of the a″ orbitals. The EDA results indicate that the latter term contributes 16.0% of the total ΔE_{orb} term. This is significantly higher than the 3.4% contribution of the a″ orbitals in **1a**, which come from the mixing of the occupied and vacant C−H and P−H orbitals.

The EDA values for **1** will now be used as reference for the other ylides **2**−**8**. For H_2C-PMe_3 we present only the results for **2a** and **2b** using the end-on model. Table 3 shows that **2a** has a larger intrinsic interaction energy ΔE_{int} (−162.5 kcal/mol)

TABLE 3: Energy Decomposition Analysis for H_2CPH_3 (1), H_2CPMe_3 (2), H_2CPF_3 (3), and $(BH_2)_2CPH_3$ (4) at BP86/TZ2P[a]

	1a side-on	**1a** end-on	**1b** end-on	**2a** end-on	**2b** end-on	**3a** end-on	**3b** end-on	**4a** end-on	**4b** end-on
ΔE_{int}	−79.1	−147.0	−139.5	−162.5	−156.7	−152.5	−150.2	−66.5	−66.4
ΔE_{Pauli} [b]	541.9	317.7	211.8	317.4	227.5	256.2	220.8	288.7	288.8
ΔE_{elstat} [b]	−274.6 (44.2%)	−158.8 (34.2%)	−97.3 (27.7%)	−172.6 (36.0%)	−122.4 (31.9%)	−117.2 (28.7%)	−97.2 (26.2%)	−132.8 (37.4%)	−132.8 (37.4%)
ΔE_{orb} [b]	−346.4 (55.8%)	−305.8 (65.8%)	−254.0 (72.3%)	−307.3 (64.0%)	−261.7 (68.1%)	−291.5 (71.3%)	−273.7 (73.8%)	−222.5 (62.6%)	−222.4 (62.6%)
$\Delta E_{orb}(a')$ [c]	−336.2 (97.1%)	−295.5 (96.6%)	−213.5 (84.0%)	−297.1 (96.7%)	−225.6 (86.2%)	−276.9 (95.0%)	−219.2 (80.1%)	−210.4 (94.6%)	−203.6 (91.6%)
$\Delta E_{orb}(a'')$ [c]	−10.2 (2.9%)	−10.4 (3.4%)	−40.5 (16.0%)	−10.2 (3.3%)	−36.2 (13.8%)	−14.6 (5.0%)	−54.5 (19.9%)	−12.1 (5.4%)	−18.8 (8.4%)
$\Delta E_{prep}(PX_3+CR_2)$	3.0 + 19.0	3.0 + 86.8	2.5 + 81.1	2.6 + 86.9	2.3 + 82.5	2.6 + 81.7	2.2 + 80.3	3.1 + 32.0	3.1 + 31.9
D_e	57.1	57.2	55.9	73.0	71.9	68.2	67.7	31.4	31.4
d(C−P)[d]	1.683	1.683	1.664	1.684	1.672	1.615	1.619	1.739	1.739

[a] Energies in kcal mol^{-1}. [b] The percentage values in parentheses give the contribution to the total attractive interactions $\Delta E_{elstat} + \Delta E_{orb}$. [c] The percentage values in parentheses give the contribution to the orbital interactions ΔE_{orb}. [d] C−P distance in Å.

than **1a** (−147.0 kcal/mol), which means that the larger BDE value that is calculated for **2a** (Table 1) arises from the stronger attraction of the fragment and not from less preparation energy. The EDA data indicate that the stronger bond in **2a** than in **1a** does *not* come from more attractive orbital interactions, but comes from stronger electrostatic attraction. The values for ΔE_{Pauli} and ΔE_{orb} are not very different between the two compounds, but the ΔE_{elstat} value for **2a** (−172.6 kcal/mol) is significantly larger than that for **1a** (−158.8 kcal/mol). The difference between the two data (13.8 kcal/mol) matches very well the difference between the BDEs at the same level of theory (15.8 kcal/mol). Note that the C−P bond distance in **2a** (1.684 Å) is nearly the same as in **1a** (1.683 Å), which shows that the stronger electrostatic attraction is not due to a shorter bond. A possible reason for the larger ΔE_{elstat} value of the former compound compared with the latter molecule could be that substitution of hydrogen by methyl yields a rehybridization of the phosphorus lone-pair orbital, which overlaps more strongly with the nucleus of the carbene carbon atom. A similar situation has recently been found for transition metal−phosphane complexes $(CO)_5M-(PX_3)$ (M = Cr, Mo, W; X = H, Me, F, Cl).[51] The compounds $(CO)_5M-(PH_3)$ and $(CO)_5M-(PMe_3)$ have larger BDE values than the halogen systems $(CO)_5M-(PF_3)$ and $(CO)_5M-(PCl_3)$, although the latter species have more attractive metal−phosphane orbital interactions. The weaker bonds come from significantly smaller ΔE_{elstat} values in the latter species because the halogen atoms yield more contracted phosphorus lone-pair orbitals.[51] The EDA results for **2b** (Table 3) suggest that the contribution of the $H_2C \rightarrow PMe_3$ π back-donation (13.8% of ΔE_{orb}) is less important than in **1b** (16.0% of ΔE_{orb}). The Wiberg bond order values indicate also a weaker double-bond character in **2a** than in **1a** (Table 2). We want to point out that the weaker double-bond character does not correlate with the pyramidalization angles of **1a** and **2a**, which have values of 146.7° and 149.3° for **1a**, but 150.6° and 153.0° for **2a** (Figure 1).

The EDA data for H_2C-PF_3 (**3**) are very interesting because they resemble the results for the above-mentioned compounds $(CO)_5M-(PX_3)$. Structure **3a** has a much smaller ΔE_{elstat} value (−117.2 kcal/mol) than **1a** (−158.8 kcal/mol) and **2a** (−172.6 kcal/mol), although the C−P bond of **3a** (1.615 Å) is clearly shorter than in **1a** (1.683 Å) and **2a** (1.684 Å). This results from the more compact phosphorus lone-pair orbital in PF_3, which, in **3a**, yields also less Pauli repulsion and overall attractive orbital interactions than in **1a** and **2a** (see the values for ΔE_{Pauli} and ΔE_{orb} in Table 3). The net effect is that the C−P bond of **3a** is weaker than in **2a** but stronger than in **1a** (see the BDE and the ΔE_{int} values in Table 3). The EDA results for **3b** show, however, that the $H_2C \rightarrow PF_3$ π back-donation (19.9% of ΔE_{orb}) is stronger than the π back-donation in **1b** and **2b**. This is reasonable because PF_3 is a better π acceptor than PH_3 and PMe_3, since the vacant PF_3 π^* orbitals are much lower in energy. The larger relative value for $\Delta E_{orb}(a'')$ is also in agreement with the Wiberg bond order, which indicates that **3a** has the highest double-bond character (Table 2). The EDA results explain why stronger $D \rightarrow PF_3$ π back-donation in $(CO)_5M-PF_3$[51] and in H_2C-PF_3 does not necessarily yield a stronger bond.

The conformations **4a** and **4b** of $(BH_2)_2C-PH_3$ are energetically nearly degenerate. The EDA data for the two species show that the latter form has weaker attraction from the a′ orbitals and equally stronger attraction from the a″ orbitals while the other terms remain constant. These can directly be used as a measure of the $(BH_2)_2C \rightarrow PH_3$ π back-donation into vacant

TABLE 4: Energy Decomposition Analysis for H_2CNH_3 (5), H_2CAsH_3 (6), H_2SiPH_3 (7), and $(BH_2)_2SiPH_3$ (8) at BP86/TZ2P[a]

	5a side-on	**5a** end-on	**5b** end-on	**6a** side-on	**6a** end-on	**6b** end-on	**7a** side-on	**7b** end-on	**8a** end-on	**8b** end-on
ΔE_{int}	−45.2	−129.2	−93.7	−57.9	−133.4	−114.2	−28.3	−81.2	−33.6	−33.9
ΔE_{Pauli}	293.8	417.5	198.2	316.6	356.4	169.7	97.0	110.5	104.9	105.2
ΔE_{elstat} [b]	−147.5 (43.5%)	−202.8 (37.1%)	−116.3 (39.9%)	−168.8 (45.1%)	−192.0 (39.2%)	−77.5 (27.3%)	−59.0 (47.1%)	−75.0 (39.1%)	−65.4 (47.2%)	−65.6 (47.2%)
ΔE_{orb} [b]	−191.5 (56.5%)	−343.8 (62.9%)	−175.5 (60.1%)	−205.7 (54.9%)	−297.7 (60.8%)	−206.5 (72.7%)	−66.3 (52.9%)	−116.7 (60.9%)	−73.1 (52.8%)	−73.5 (52.8%)
$\Delta E_{orb}(a')$[c]	−186.4 (97.3%)	−338.9 (98.6%)	−158.7 (90.4%)	199.2 (96.8%)	−291.1 (97.8%)	−179.2 (86.8%)	−61.4 (92.6%)	−84.9 (72.7%)	−68.6 (93.8%)	−64.0 (87.0%)
$\Delta E_{orb}(a'')$[c]	−5.2 (2.7%)	−4.9 (1.4%)	−16.9 (9.6%)	−6.5 (3.2%)	−6.6 (2.2%)	−27.3 (13.2%)	−4.9 (7.4%)	−31.8 (27.3%)	−4.6 (6.3%)	−9.6 (13.0%)
$\Delta E_{prep}(E^2H_3 + E^1R_2)$	0.7 + 16.1	0.7 + 100.1	0.9 + 73.4	3.4 + 17.4	3.4 + 92.9	3.6 + 77.1	1.2 + 0.2	2.4 + 82.1	1.9 + 6.6	1.9 + 6.7
D_e	28.4	28.4	19.4	37.1	37.1	33.5	26.9	−3.3	25.1	25.3
$d(E^1-E^2)$[d]	1.543	1.543	1.459	1.846	1.846	1.789	2.328	2.142	2.302	2.301

[a] Energies in kcal mol^{-1}. [b] The percentage values in parentheses give the contribution to the total attractive interactions $\Delta E_{elstat} + \Delta E_{orb}$. [c] The percentage values in parentheses give the contribution to the orbital interactions ΔE_{orb}. [d] E^1-E^2 distance in Å.

PH_3 π^* MOs which appear in **4a** from the C−B bonding orbitals, while in **4b** they come from the carbon lone-pair MO. The results in Table 3 suggest that the $(BH_2)_2C \rightarrow PH_3$ π back-donation in **4b** contributes only 8.4% of the total orbital attraction, which is much less than in **1b**−**3b**. The weaker π back-donation $(BH_2)_2C \rightarrow PH_3$ compared with $H_2C \rightarrow PH_3$ in **1b** (16.0%) can be explained with the competing π acceptance of the boron atoms. The NBO analysis[52] shows that the p(π) atomic orbital (AO) of each boron atom in **4b** is occupied by 0.24 e (0.23 in **4a**), which means that the total $C \rightarrow B_2$ π donation is 0.48 e. The comparatively small $(BH_2)_2C \rightarrow PH_3$ π-bonding contribution, which is calculated by the EDA, agrees with the Wiberg bond order of only 1.107 (Table 2) for $(BH_2)_2C-PH_3$ (**4b**).

Table 4 gives the EDA results of the ylides **5**−**8**. The values for the methylene compounds H_2C-NH_3 (**5**) and H_2C-AsH_3 (**6**) will be compared with the result for the phosphorus ylide H_2C-PH_3 (**1**) (Table 3). In the latter compound (**1**), the end-on approach was found to provide a better model for the bonding in the equilibrium structure **1a**, because the Pauli repulsion and the orbital interaction are smaller than in the side-on model. The EDA data for **5a** and **6a** exhibit the opposite behavior; i.e., the side-on model gives smaller absolute values for ΔE_{Pauli} and ΔE_{orb} than the end-on model. The smaller BDE values for **5a** and **6a** arise from the intrinsic $H_2C-E^2H_3$ interaction energy ΔE_{int}, which follows the trend N < As < P (Tables 3 and 4). The trend does not correlate with a particular change of the contributions of ΔE_{elstat} and ΔE_{orb} to the bonding interactions in $H_2C-E^2H_3$. The relative contributions of the attractive terms to the bonding interactions in **1a**, **5a**, and **6a** are nearly the same. The Wiberg bond orders suggest (Table 2) that the trend of the bond strength may be related to the π contribution to the $H_2C-E^2H_3$ orbital interactions. To estimate the strength of the carbon lone-pair $H_2C \rightarrow E^2H_3$ π back-donation, we must compare the EDA results for **1b**, **5b**, and **6b** using the end-on model. This may be criticized because the conformation **5b** is 9.0−9.5 kcal/mol higher in energy than **5a**. However, the value for $\Delta E_{orb}(a'')$ in **5a**, which has a significantly shorter C−N bond than **5b**, may be used as an upper bound for the intrinsic π back-donation in H_2C-NH_3. The EDA data show that the relative contributions of $\Delta E_{orb}(a'')$ follow the order **5b** (9.6%) < **6b** (13.2%) < **1b** (16.0%). Since the value for **5b** overestimates the π back-donation in H_2C-NH_3 (so does to a lesser extent the value for **6b**), we conclude that the weaker $H_2C-E^2H_3$ bonds in the nitrogen and arsenic homologues of H_2C-PH_3 are caused by the weaker π back-donation.

The equilibrium geometry of H_2Si-PH_3 (**7a**) reveals that the side-on approach of the fragments is the appropriate model for the EDA calculations. The calculated data given in Table 4 agree with this conclusion. The calculated energy terms for the side-on model are much smaller than those for the end-on model. A comparison of the EDA values for H_2Si-PH_3 (**7a**) with H_2C-PH_3 (**1a**) shows that the weaker bonding in the former compound reflects the intrinsically less strongly bonded third-row atom Si compared with the second-row atom C. The reason for this has been discussed in detail by Kutzelnigg.[53] Although the end-on model is clearly not appropriate for describing the bonding in **7a**, we carried out EDA calculations of the latter for the energetically high-lying conformation **7b** in order to investigate the intrinsic π-donor strength of the p(π) electron lone pair of Si. Table 4 shows that the relative contribution of $\Delta E_{orb}(a'')$ is rather large (27.3% of ΔE_{orb}), which means that the p(π) orbital of Si is a potentially strong π donor. This is not surprising, because the orbital is energetically rather high

TABLE 5: Eigenvalues of the Fermi Holes in $E^1H_2E^2X_3$ (E^1 = C, Si; E^2 = P, N, As; X = H, F)[a]

molecule	no.	fragment	eigenvalue	degeneracy	interpretation
CH_2PH_3	**1a**	CH_2	~2	1	C 1s
			~2	2	C−H σ bond
			1.692	1	delocalized p lone pair on C
			1.339	1	C−P σ bond
		PH_3	~2	1	P 1s
			~2	1	P 2s
			~2	3	P 2p
			~2	3	P−H σ bond[b]
			0.661	1	C−P σ bond
			0.308	1	delocalized p lone pair on C
CH_2PF_3	**3a**	CH_2	~2	1	C 1s
			~2	2	C−H σ bond
			1.662	1	delocalized p lone pair on C
			1.407	1	C−P σ bond
		PF_3	~2	3	P−F σ bond[c]
			0.593	1	C−P σ bond
			0.337	1	delocalized p lone pair on C
CH_2NH_3	**5a**	CH_2	~2	1	C 1s
			~2	2	C−H σ bond
			1.847	1	delocalized p lone pair on C
			0.450	1	C−N σ bond
		NH_3	~2	3	N−H σ bond[d]
			1.550	1	C−N σ bond
			0.152	1	delocalized p lone pair on C
CH_2AsH_3	**6a**	CH_2	~2	1	C 1s
			~2	2	C−H σ bond
			1.685	1	delocalized p lone pair on C
			0.934	1	C−As σ bond
		AsH_3	~2	3	As−H σ bond[e]
			1.066	1	C−As σ bond
			0.315	1	delocalized p lone pair on C
SiH_2PH_3	**7a**	SiH_2	~2	1	Si 1s
			~2	1	Si 2s
			~2	3	Si 2p
			~2	2	Si−H σ bond
			1.800	1	delocalized p lone pair on Si
			0.319	1	C−P σ bond
		PH_3	~2	3	P−H σ bond[f]
			1.680	1	Si−P σ bond
			0.196	1	delocalized p lone pair on Si

[a] The holes associated with core orbitals and with the fluorine lone-pair orbitals are not shown. [b] There are two different P−H bonds. The eigenvalues differ only by ~0.037. [c] There are two different P−F bonds. The eigenvalues differ only by ~0.015. [d] There are two different N−H bonds. The eigenvalues differ only by ~0.019. [e] There are two different As−H bonds. The eigenvalues differ only by ~0.021. [f] There are two different P−H bonds. The eigenvalues differ only by ~0.008.

lying. However, it requires much energy to enforce a geometry with a planar arrangement around the silicon atom, which would lead to strong $H_2Si \rightarrow PH_3$ π back-donation. The reason is that in the equilibrium geometry **7a** the silicon lone-pair orbital becomes mainly a 3s AO, which is much lower in energy than a 3p AO. It has been shown that s/p hybridization of heavier main-group atoms is not favorable because of the much larger spatial separation compared with the 2s/2p hybridization of first octal-row atoms.[53]

A planar arrangement around the silicon atom has, however, been achieved in $(BH_2)_2Si-PH_3$ (**8**), where the driving force is the partial delocalization of the silicon p(π) orbital into the vacant orbitals of boron. The NBO analysis of **8b** gives a p(π) occupation at each boron atom of 0.33 e (0.32 e in **8a**), which is even more than the p(π) occupation at the boron atoms in $(BH_2)_2C-PH_3$ (**4**). The EDA results for the equilibrium structure **8b** show that the $(BH_2)_2Si \rightarrow PH_3$ π donation contributes 13.0% of the orbital interactions (Table 4). This is approximately twice as strong as the hyperconjugative π interaction in **8a**, which is energetically nearly degenerate with **8b**. Note that the Si−P bond in **8a** and **8b** is significantly shorter than in **7a**, but longer than in **7b**, which is in agreement with the EDA data for the relative strength of the $\Delta E_{orb}(a'')$ contribution. The values for the BDE in the equilibrium structures **7a** and **8b** are nearly the same.

The EDA information about the energy contributions to the $R_2E^1-E^2X_3$ bond will now be complemented with the DAFH results for the equilibrium structures of CH_2PH_3 (**1a**), CH_2PF_3 (**3a**), CH_2NH_3 (**5a**), CH_2AsH_3 (**6a**), and SiH_2PH_3 (**7a**). The compounds H_2CPMe_3 (**2**), $(BH_2)_2CPH_3$ (**4**), and $(BH_2)_2SiPH_3$ (**8**) have not been investigated with the DAFH method because the integration over the atomic basins of the substituents is too time-consuming, and we think that the information from the calculated data of **1a**, **3a**, **5a**, **6a**, and **7a** is sufficient for the purpose of this work. The numerical results of the DAFH calculations are given in Table 5. Some DAFH eigenvectors for **1a** and **7a** which are pertinent for the discussion are shown in Figures 3 and 4.

We begin the discussion of the DAFH results with the calculated data of the fragments CH_2 and PH_3 of the ylide **1a** (Table 5). For the CH_2 fragment there are two eigenvectors with eigenvalues of 1.692 and 1.339, besides the C 1s core and the two C−H σ bonds which have eigenvalues of ~2. The former eigenvectors are easily identified by visual inspection of the shapes as the carbon electron lone pair being delocalized to a certain extent toward the PH_3 fragment, thus contributing to the C−P bond (Figure 3b), and as the genuine C−P σ bond (Figure 3c). The eigenvalues for PH_3 are complementary to the eigenvalues for CH_2. There are 10 core electrons at P and six

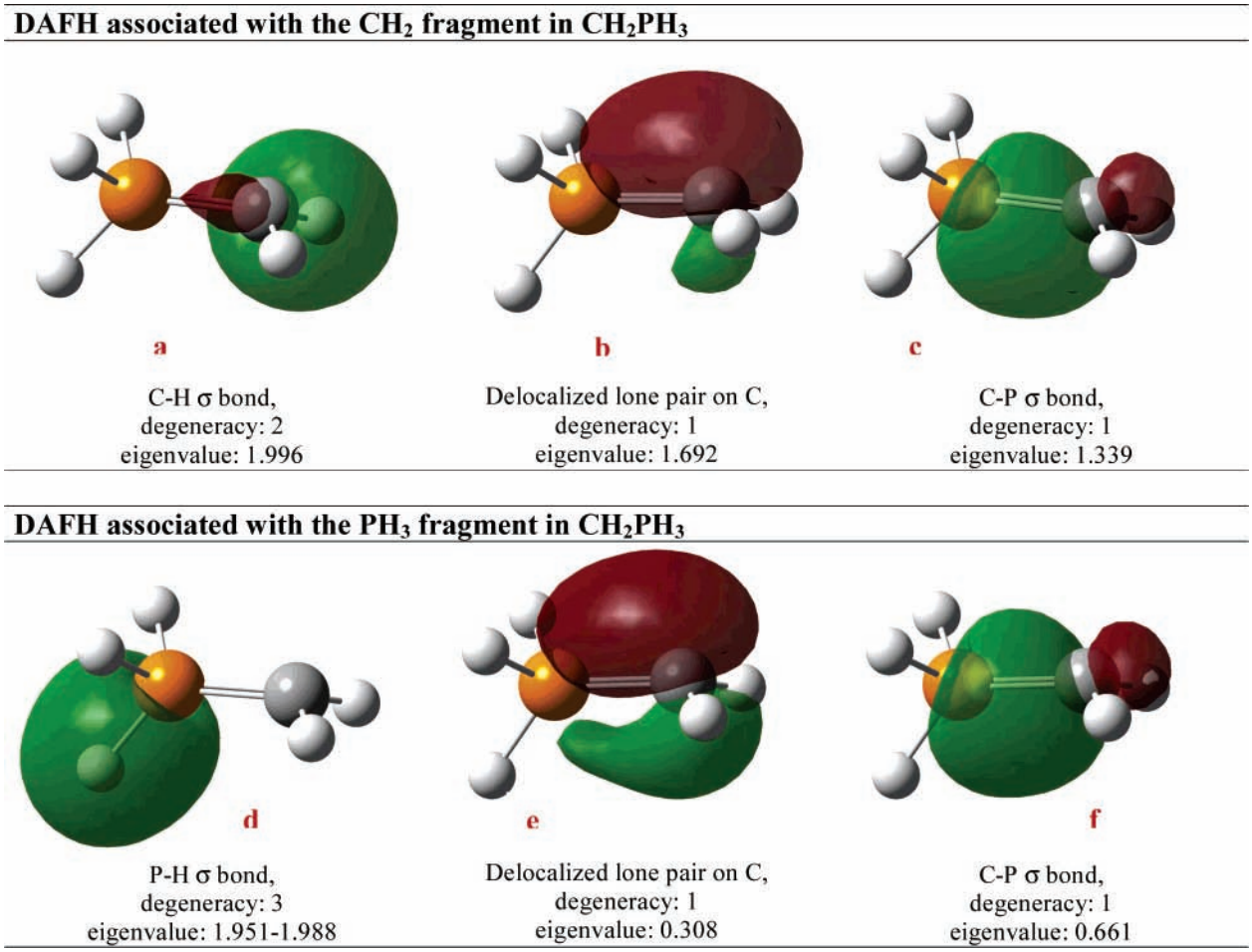

Figure 3. Eigenvectors of the domain-averaged Fermi holes associated with the CH_2 and PH_3 fragments in CH_2PH_3 (**1a**, isovalues 0.055).

electrons for the P−H σ bonds which are identified as eigenvectors with values of ∼2 (Table 5). The PH_3 part of the C−P σ bond has an eigenvalue of 0.661, while the delocalized lone pair of the methylene fragments yields an eigenvector with the eigenvalue 0.308. The shape of the latter eigenvectors is also shown in Figure 3. The small value 0.308 for the back-donation eigenvector at PH_3 is in agreement with the EDA results, which suggest that the π back-donation is not very strong. It is interesting, however, that the eigenvalue of the eigenvector associated with the P−C σ bond has a larger value at CH_2 (1.339) than at PH_3 (0.661). This means that, although the P−C σ bond comes from the donation of the phosphorus lone-pair orbital into the empty carbene orbital, it has eventually its greatest extension at carbon rather than at phosphorus. Note that C is more electronegative (2.5) than P (2.1) and that there is a concomitant C → P back-donation. The larger eigenvalue of the DAFH eigenvectors for the P−C σ bonding orbital at the carbon side is supported by the NBO results. The P−C bonding orbital of CH_2PH_3 (**1a**) is polarized toward the carbon atom (54%) rather than the phosphorus atom (46%).

The comparison between the DAFH results for **1a** and **3a** shows that the delocalization of the carbon lone pair becomes as expected stronger in CH_2PF_3 than in CH_2PH_3, because PF_3 is a better π-acceptor. This becomes obvious from the calculated eigenvalues for the respective eigenvectors which have values of 1.692 (**1a**) and 1.662 (**3a**) at the CH_2 fragment. The polarization of the eigenvector belonging to the P−C bond toward carbon in **3a**, given by the eigenvalues at methylene, is slightly larger (1.407) than in **1a** (1.339).

The DAFH results for the nitrogen and arsenic, in homologues CH_2NH_3 (**5a**) and CH_2AsH_3 (**6a**), exhibit significant differences from those for the phosphorus ylide CH_2PH_3 (**1a**). The eigenvector of the CH_2 fragment of **5a**, which is associated with the C−N bond, has an eigenvalue of only 0.450 (Table 5), meaning that the extension at the carbon site is now rather small. Furthermore, the eigenvector of the same fragment which belongs to the carbon lone pair has a value of 1.847. This suggests that there is little back-bonding character in **5a**, in agreement with the EDA results. The back-bonding character of the electronic structure in CH_2AsH_3 (**6a**) is comparable to the situation in **1a**. This becomes obvious by the calculated eigenvalues for the respective eigenvector of the CH_2 fragments in **6a** (1.685) and **1a** (1.692). There is a large difference, however, between the DAFH results for the C−P and C−As bonds. The eigenvalues of the associated eigenvectors of **6a** for the fragments CH_2 (0.934) and AsH_3 (1.066) suggest a nearly unpolar C−As bond, while the C−P bond of **1a** is clearly polarized toward the carbon end. This indicates that the phosphorus homologues have an ylidic bond which is different from the nitrogen and arsenic homologues.

The numerical DAFH results given in Table 5 indicate that the electronic structure concerning the Si−P bonding in SiH_2PH_3 (**7a**) is similar to that in CH_2NH_3 (**5a**). We want to point out that the DAFH results give insight into the electronic structure and particularly into the bonding of the molecules, while the EDA sheds light on the energy contributions to the bond. This has to be considered when the results of the two methods are compared with each other. Nevertheless, the EDA

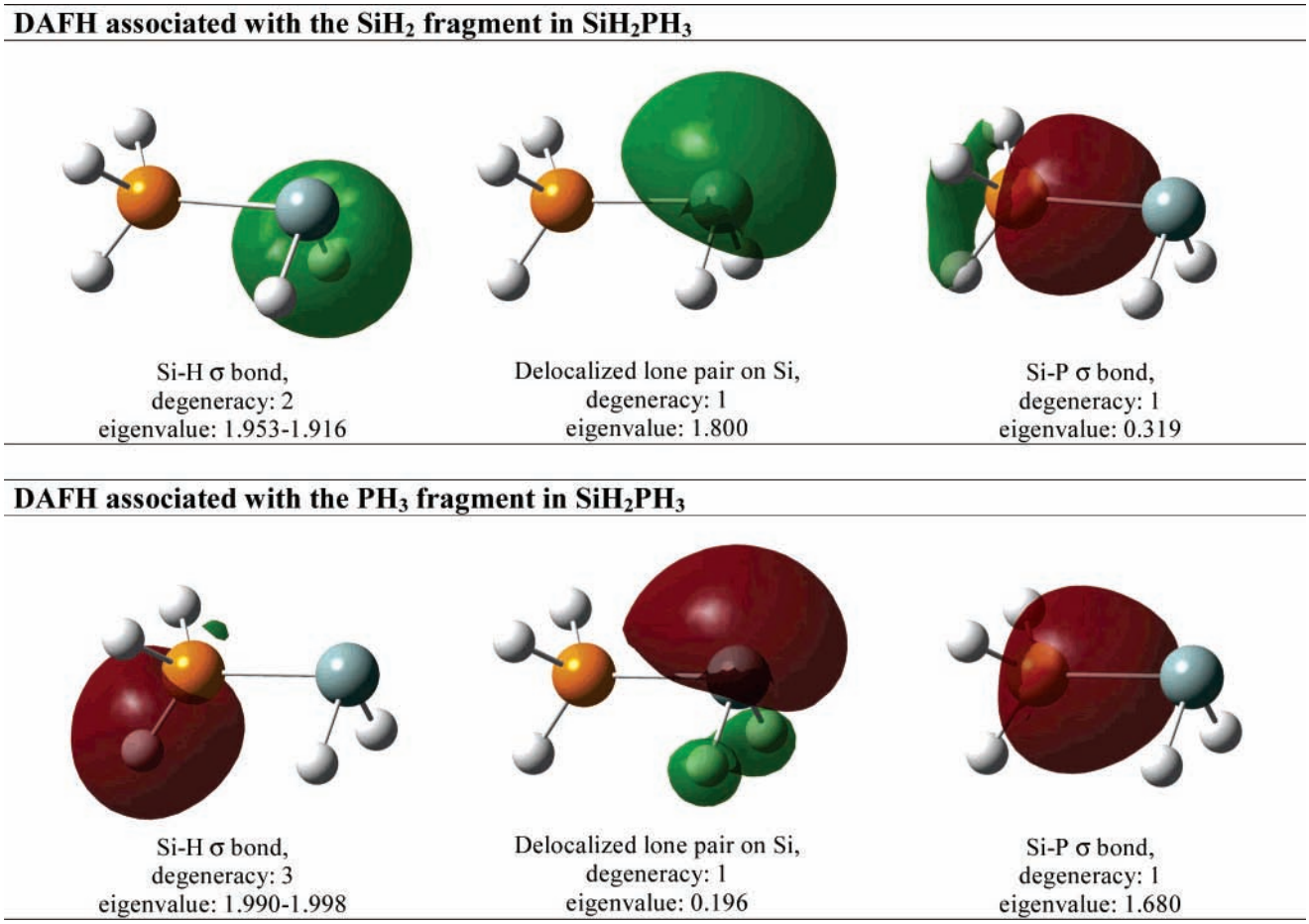

Figure 4. Eigenvectors of the domain-averaged Fermi holes associated with the SiH_2 and PH_3 fragments in SiH_2PH_3 (**7a**, isovalues 0.055).

results show also that the relative contributions of the energy terms, which are given by the EDA for **5a** and **7a**, are very similar to each other (Table 3). Figure 4 shows that the eigenvectors associated with the σ bonds and with the π back-donation are more localized in **7a** at P and Si, while they are more delocalized in **1a** over P and C.

The analysis of the bonding situation in the phosphorus ylides may be compared with our recent investigation of carbodiphosphoranes $C(PR_3)_2$.[54] In the latter class of compounds there are two donor−acceptor bonds between phosphorus and carbon C ← PR_3, but there is no significant back-donation from carbon to phosphorus. The valence electrons of carbon remain as electron lone pairs which leads to unusual molecules such as dications $[H_2C(PR_3)_2]^{2+}$ where two protons are attached to the same carbon atom[55] and a trication $[\{(Ph_3P)_2CH\}_2Ag]^{3+}$ where the carbon atom carries a highly negative partial charge of −1.34 e.[54] The phosphorus−carbon bond in phosphorus ylides $R_2C(PR'_3)$ also has a $R_2C \leftarrow PR'_3$ donor−acceptor component between phosphorus and carbon, but there is a significant back-donation $R_2C \rightarrow PR'_3$ whose contribution is fine-tuned by the nature of the ligands R and R′.

Summary

The analyses of the $R_2E^1-E^2X_3$ compounds using charge and energy partitioning methods show that the peculiar features of the ylidic bond can be understood in terms of donor and acceptor interactions between closed-shell R_2E^1 and E^2X_3 fragments. The DAFH analysis clearly shows that there are two electron-pair bonding contributions to the ylidic bond. The strength of the donor and acceptor contributions to the attractive orbital interactions may be quantitatively estimated from the EDA calculations, which give also the contributions of the electrostatic attraction and the Pauli repulsion of the chemical bonding. The EDA and DAFH results clearly show that the orbital interactions take place through the singlet ground state of the R_2E^1 fragment, where the donor orbital of E^1 yields the π-type back-donation, while the E^2X_3 lone-pair orbital yields the σ-type bonding. Both bonds are polarized toward R_2E^1 when $E^2 = P$, while the σ-type bonding remains more polarized at E^2X_3 when $E^2 = N$, As. This shows that the phosphorus ylides exhibit a particular bonding situation which is clearly different from that of the nitrogen and arsenic homologues. With ylides built around a P−C linkage, the π-acceptor strength of phosphorus and the σ-acceptor strength at carbon contribute to a double bond which is enhanced by electrostatic contributions. The strength of the σ and π components and the electrostatic attraction are then fine-tuned by the substituents at C and P, which yields a peculiar type of carbon−phosphorus bonding. The EDA data show that, while the relative strength of the ylidic bond is predominantly determined by the $R_2E^1 \rightarrow E^2X_3$ π back-donation, the electrostatic contribution to the bonding is also an important factor. The calculations of the $R_2E^1-E^2X_3$ bond dissociation energy using ab initio methods give the order $H_2C-PMe_3 > H_2CPF_3 > H_2CPH_3 > (BH_2)_2CPH_3 > H_2CAsH_3 > H_2CNH_3 \sim H_2SiPH_3 \sim (BH_2)_2SiPH_3$. The DFT methods underestimate the bond strength of $(BH_2)_2CPH_3$.

Acknowledgment. We are grateful to the referees for helpful comments and suggestions. M.J.C. acknowledges FCT (Grant SFRH/BSAB/407/2004). This work was supported by the Deutsche Forschungsgemeinschaft. Excellent service by the

Hochschulrechenzentrum of the Philipps-Universität Marburg is gratefully acknowledged. Additional computer time was provided by the HLRS Stuttgart and HHLRZ Darmstadt.

Supporting Information Available: Table S1 with the optimized coordinates and total energies of the molecules. Table S2 with the EDA results of **1**−**8** using triplet fragments. This material is available free of charge via the Internet at http://pubs.acs.org.

References and Notes

(1) Naito, T.; Nagase, S.; Yamataka, H. *J. Am. Chem. Soc.* **1994**, *116*, 10080.
(2) Chauvin, R. *Eur. J. Inorg. Chem.* **2000**, 577.
(3) Schmidbaur, H.; Jeong, J.; Schier, A.; Graf, W.; Wilkinson, D. L.; Müller, G. *New J. Chem.* **1989**, *13*, 341.
(4) Allen, F. H. *Acta Crystallogr.* **2002**, *B58*, 380.
(5) Bruno, I. J.; Cole, J. C.; Edginton, P. R.; Kessler, M.; Macrae, C. F.; McCabe, P.; Pearson, J.; Taylor, R. *Acta Crystallogr.* **2002**, *B58*, 389.
(6) Mitzel, N. W.; Brown, D. H.; Parsons, S.; Brain, P. T.; Pulham, C. R.; Rankin, D. W. H. *Angew. Chem., Int. Ed.* **1998**, *37*, 1670.
(7) Mitchell, K. A. R. *Chem. Rev.* **1969**, *69*, 157.
(8) Nuslászi, L.; Veszprémi, T.; Réffy, J. *J. Chem. Phys.* **1995**, *99*, 10142.
(9) Bader, R. F. W. *Atoms in Molecules: A Quantum Theory*; University of Oxford Press: Oxford, 1990.
(10) (a) Mitrasinovic, P. M. *J. Comput. Chem.* **2001**, *22*, 1387. (b) Mitrasinovic, P. M. *J. Phys. Chem. A* **2002**, *106*, 7026. (c) Mitrasinovic, P. M. *Chem. Phys.* **2003**, *286*, 1.
(11) Dobado, J. A.; Martínez-García, H.; Molina Molina, J.; Sundberg, M. R. *J. Am. Chem. Soc.* **2000**, *122*, 1144.
(12) Sanchez-Gonzalez, A.; Martinez-Garcia, H.; Melchor, S.; Dobado, J. A. *J. Phys. Chem. A* **2004**, *108*, 9188.
(13) Dransfeld, A.; Forro, A.; Veszpremi, T.; Flock, M.; Nguyen, M. T. *J. Chem. Soc., Perkin Trans. 2* **2000**, 2475.
(14) Noury, S.; Silvi, B.; Gillespie, R. J. *Inorg. Chem.* **2002**, *41*, 2164.
(15) Chamorro, A.; Fuentealba, P.; Savin, A. *J. Comput. Chem.* **2003**, *24*, 496.
(16) Power, P. P. *Chem. Rev.* **1999**, *99*, 3463.
(17) Gilheany, D. G. *Chem. Rev.* **1994**, *94*, 1393.
(18) (a) Morokuma, K. *J. Chem. Phys.* **1971**, *55*, 1236. (b) Kitaura, K.; Morokuma, K. *Int. J. Quantum Chem.* **1976**, *10*, 325.
(19) (a) Ziegler, T. Rauk, A. *Theor. Chim. Acta* **1977**, *46*, 1. (b) Ziegler, T.; Rauk, A. *Inorg. Chem.* **1979**, *18*, 1755. (c) Ziegler, T.; Rauk, A. *Inorg. Chem.* **1979**, *18*, 1558.
(20) (a) Bickelhaupt, F. M.; Baerends, E. J. In *Reviews in Computational Chemistry*; Lipkowitz, K. B., Boyd D. B., Eds.; Wiley-VCH: New York, 2000; Vol. 15, p 1. For reviews about EDA applications, see: (b) Lein, M.; Frenking, G. In *Theory and Applications of Computational Chemistry: The First 40 Years*; Dykstra, C. E., Frenking, G., Kim, K. S., Scuseria, G. E., Eds.; Elsevier: Amsterdam, 2005; p 367. (c) Frenking, G.; Wichmann, K.; Fröhlich, N.; Loschen, C.; Lein, M.; Frunzke, J.; Rayón, V. M. *Coord. Chem. Rev.* **2003**, *238*−*239*, 55.
(21) Ponec, R.; Duben, J. *J. Comput. Chem.* **1999**, *8*, 760.
(22) Ponec, R.; Girones, X. *J. Phys. Chem. A* **2002**, *106*, 9506.
(23) Ponec, R.; Roithova, J. *Theor. Chem. Acc.* **2001**, *105*, 383.
(24) Ponec, R.; Yuzhakov, G.; Girones, X.; Frenking, G. *Organometallics* **2004**, *23*, 1790.
(25) Becke, A. D. *J. Chem. Phys.* **1993**, *98*, 5648.
(26) Stephens, P. J.; Devlin, J. F.; Chabalowski, C. F.; Frisch, M. J. *J. Phys. Chem.* **1994**, *98*, 11623.
(27) Lee, C.; Yang, W.; Parr, R. G. *Phys. Rev. B* **1988**, *37*, 785.
(28) Møller, C.; Plesset, M. S. *Phys. Rev.* **1934**, *46*, 618.
(29) (a) Woon, D. E.; Dunning, T. H., Jr. *J. Chem. Phys.* **1993**, *98*, 1358. (b) Davidson, E. R. *Chem. Phys. Lett.* **1996**, *260*, 514. (c) Dunning, T. H., Jr. *J. Chem. Phys.* **1989**, *90*, 1007. (d) Kendall, R. A.; Dunning, T. H., Jr. Harrison, R. J. *J. Chem. Phys.* **1992**, *96*, 6796. (e) Peterson, K. A.; Woon, D. E.; Dunning, T. H., Jr. *J. Chem. Phys.* **1994**, *100*, 7410. (f) Wilson, A.; van Mourik, T.; Dunning, T. H., Jr. *J. Mol. Struct. (THEOCHEM)* **1997**, *388*, 339.
(30) Frisch, M. J.; Trucks, G. W.; Schlegel, H. B.; Scuseria, G. E.; Robb, M. A.; Cheeseman, J. R; Montgomery, J. A., Jr.; Vreven T.; Kudin, K. N.; Burant, J. C.; Millam, J. M.; Iyengar, S. S.; Tomasi, J.; Barone, V.; Mennucci, B.; Cossi, M.; Scalmani, G.; Rega, N.; Petersson, G. A.; Nakatsuji, H.; Hada, M.; Ehara, M.; K. Toyota, M.; Fukuda, R.; Hasegawa, J.; Ishida, M.; Nakajima, T.; Honda, Y.; Kitao, O.; Nakai, H.; Klene, M.; Li, X.; Knox, J. E.; Hratchian, H. P.; Cross, J. B.; Bakken, V.; Adamo, C.; Jaramillo, J.; Gomperts, R.; Stratmann, R. E.; Yazyev, O.; Austin, A. J.; Cammi, R.; Pomelli, C.; Ochterski, J. W.; Ayala, P. Y.; Morokuma, K.; Voth, G. A.; Salvador, P.; Dannenberg, J. J.; Zakrzewski, V. G.; Dapprich, S.; Daniels, A. D.; Strain, M. C.; Farkas, O.; Malick, D. K.; Rabuck, A. D.; Raghavachari, K.; Foresman, J. B.; Ortiz, J. V.; Cui, Q.; Baboul, A. G.; Clifford, S.; Cioslowski, J.; Stefanov, B. B.; Liu, G.; Liashenko, A.; Piskorz, P.; Komaromi, I.; Martin, R. L.; Fox, D. J.; Keith, T.; Al-Laham, M. A.; Peng, C. Y.; Nanayakkara, A.; Challacombe, M.; Gill, P. M. W.; Johnson, B.; Chen, W.; Wong, M. W.; Gonzalez, C.; Pople, J. A. *Gaussian 03*, revision B.05; Gaussian, Inc.: Wallingford, CT, 2004.
(31) (a) Montgomery, J. A.; Frisch, M. J.; Ochterski, J.; Peterson, K. A. *J. Chem. Phys.* **1999**, *110*, 2822. (b) Montgomery, J. A.; Frisch, M. J.; Ochterski, J.; Peterson, K. A. *J. Chem. Phys.* **2000**, *112*, 6532.
(32) *ADF2003.01*; Theoretical Chemistry, Vrije Universiteit, SCM: Amsterdam, The Netherlands; http://www.scm.com.
(33) Te Velde, G.; Bickelhaupt, F. M.; Baerends, E. J.; Fonseca Guerra, C.; Van Gisbergen, S. J. A.; Snijders, J. G.; Ziegler, T. *J. Comput. Chem.* **2001**, *22*, 931.
(34) Bickelhaupt, F. M.; Nibbering, N. M. M.; van Wezenbeek, E. M.; Baerends, E. J. *J. Phys. Chem.* **1992**, *96*, 4864.
(35) Becke, A. D. *Phys. Rev. A* **1988**, *38*, 3098.
(36) Perdew, J. P. *Phys. Rev. B* **1986**, *33*, 8822.
(37) Snijders, J. G.; Baerends, E. J. *At. Data Nucl. Data Tables* **1982**, *26*, 483.
(38) van Lenthe, E.; Baerends, E. J. *J. Comput. Chem.* **2003**, *24*, 1142.
(39) (a) Chang, C.; Pelissier, M.; Durand, Ph. *Phys. Scr.* **1986**, *34*, 394. (b) Heully, J.-L.; Lindgren, I.; Lindroth, E.; Lundquist, S.; Martensson-Pendrill, A.-M. *J. Phys. B* **1986**, *19*, 2799. (c) van Lenthe, E.; Baerends, E. J.; Snijders, J. G. *J. Chem. Phys.* **1993**, *99*, 4597. (d) van Lenthe, J. G.; Baerends, E. J.; Snijders, J. G. *J. Chem. Phys.* **1996**, *105*, 6505. (e) van Lenthe, E.; van Leeuwen, R.; Baerends, E. J.; Snijders, J. G. *Int. J. Quantum Chem.* **1996**, *57*, 281.
(40) Baerends, E. J.; Ellis, D. E.; Ros, P. *Chem. Phys.* **1973**, 41.
(41) Krijn, J.; Baerends, E. J. *Fit Functions in the HFS-Method, Internal Report*; Vrije Universiteit Amsterdam: Amsterdam, The Netherlands, 1984 (in Dutch).
(42) Girones, X.; Ponec, R.; Roithova, J. *WBader 1.0*; 2000.
(43) Bader, R. F. W. *AIMPAC 95*; McMaster University: Hamilton, ON, Canada.
(44) Frisch, M. J.; Trucks, G. W.; Schlegel, H. B.; Scuseria, G. E.; Robb, M. A.; Cheeseman, J. R.; Zakrzewski, V. G.; Montgomery, J. A.; Stratmann, R. E.; Burant, J. C.; Dapprich, S.; Millam, J. M.; Daniels, A. D.; Kudin, K. N.; Strain, M. C. Farkas, O.; Tomasi, J.; Barone, V.; Cossi, M.; Cammi, R.; Mennucci, B.; Pomelli, C.; Adamo, C.; Clifford, S.; Ochterski, J.; Petersson, G. A.; Ayala, P. Y.; Cui, Q.; Morokuma, K.; Malick, D. K.; Rabuck, A. D.; Raghavachari, K.; Foresman, J. B.; Cioslowski, J.; Ortiz, J. V.; Stefanov, B. B.; Liu, G.; Liashenko, A.; Piskorz, P.; Komaromi, I.; Gomperts, R.; Martin, R. L.; Fox, D. J.; Keith, T M.; Gill, P. M. W.; Johnson, B.; Chen, W.; Wong, M. W.; Andres, J. L.; Gonzalez, C.; Head-Gordon, M.; Replogle, E. S.; Pople, J. A. *Gaussian 98*, revision A7; Gaussian Inc.: Wallingford, CT, 1999.
(45) Fau, S.; Frenking, G. *J. Mol. Struct. (THEOCHEM)* **1995**, *338*, 117.
(46) Jemmis, E. D.; Subramanian, G.; Srinivas, G. N. *J. Am. Chem. Soc.* **1992**, *114*, 7939.
(47) Subramanian, G.; Jemmis, E. D. *Chem. Phys. Lett.* **1992**, *200*, 567.
(48) Wiberg, K. B. *Tetrahedron* **1968**, *24*, 1083.
(49) The values have been calculated at the same level of theory as for **1**−**8**, e.g., B3LYP/aug-cc-pVTZ.
(50) Kalemos, A.; Dunning, T. H., Jr.; Mavridis, A.; Harrison, J. F. *Can. J. Chem.* **2004**, *82*, 684.
(51) Frenking, G.; Wichmann, K.; Fröhlich, N.; Grobe, J.; Golla, W.; Le Van, D.; Krebs, B.; Läge, M. *Organometallics* **2002**, *21*, 2921.
(52) Reed, A. E.; Curtiss, L. A.; Weinhold, F. *Chem. Rev.* **1988**, *88*, 899.
(53) Kutzelnigg, W. *Angew. Chem.* **1984**, *96*, 262; *Angew. Chem., Int. Ed. Engl.* **1984**, *23*, 272.
(54) Tonner, R.; Öxler, F.; Neumüller, B.; Petz, W.; Frenking, G. *Angew. Chem.* **2006**, *118*, 8206; *Angew. Chem., Int. Ed.* **2006**, *45*, 8038.
(55) (a) Walker, J. D.; Poli, R. *Polyhedron* **1989**, *8*, 1293. (b) Jensen, W. P.; Gehrke, H.; Jones, D. R.; Suh, I.-H.; Jacobson, R. A. Z. *Kristallogr.* **1996**, *211*, 829.